Novel "3-D spacer" all fibre piezoelectric textiles for energy harvesting applications

Novel “3-D spacer” all fibre piezoelectric textiles for energy harvesting applications

Navneet Soin,[a] Tahir H. Shah,[a] Subhash C. Anand,[a] Junfeng Geng,[a] Wiwat Pornwannachai,[a] Pranab Mandal,[b] David Reid,[c] Surbhi Sharma,[d] Ravi L. Hadimani,[e] Derman Vatansever Bayramol,[f] and Elias Siores[a]*

[a]Institute for Materials Research and Innovation (IMRI), Knowledge Centre for Materials Chemistry (KCMC), University of Bolton, Deane Road, BL3 5AB, United Kingdom

[b]Department of Chemistry, University of Liverpool, Liverpool L69 7ZD, Merseyside, United Kingdom

[c]Department of Chemistry, University of Cambridge, Cambridge, CB2 1EW, United Kingdom

[d]Department of Chemical Engineering, University of Birmingham, Edgbaston, Birmingham, B15 2TT, United Kingdom

[e]Department of Electrical and Computer Engineering, Iowa State University, Ames, Iowa 50011, United States of America

[f]Department of Textile Engineering, Namik Kemal University, Corlu-Tekirdag, 59860, Turkey

* Author Email Address n.soin@bolton.ac.uk

Institute of Materials Research and Innovation (IMRI), Knowledge Centre for Materials Chemistry (KCMC), University of Bolton, Bolton, Deane Road, BL3 5AB, United Kingdom

Telephone +44(0) 1204903118

Abstract

The piezoelectric effect in Poly(vinylidene fluoride), PVDF, was discovered over four decades ago and since then, significant work has been carried out aiming at the production of high β-phase fibres and their integration into fabric structures for energy harvesting. However, little work has been done in the area of production of *"true piezoelectric fabric structures"* based on flexible polymeric materials such as PVDF. In this work, we demonstrate "3D spacer" technology based all-fibre piezoelectric fabrics as power generators and energy harvesters. The knitted single-structure piezoelectric generator consists of high β-phase (~80%) piezoelectric PVDF monofilaments as the spacer yarn interconnected between silver (Ag) coated polyamide multifilament yarn layers acting as the top and bottom electrodes. The novel and unique textile structure provides an output power density in the range of 1.10 - 5.10 μWcm^{-2} at applied impact pressures in the range of 0.02 - 0.10 MPa, thus providing significantly higher power outputs and efficiencies over the existing 2D woven and nonwoven piezoelectric structures. The high energy efficiency, mechanical durability and comfort of the soft, flexible and all-fibre based power generator is highly attractive for a variety of potential applications such as wearable electronic systems and energy harvesters charged from ambient environment or by human movement.

Keywords: Poly(vinylidene fluoride) PVDF, β phase, piezo force microscopy, all-fibre soft generators, energy harvesting, piezoelectric effect

Introduction

The harvesting of waste energy from ambient environment and human movement has long been considered as an attractive alternative over traditional rechargeable batteries for providing electrical power to low-energy consumption devices such as wireless body worn sensors and wearable consumer electronics [1-3]. The battery technology and indeed the energy harvesting technology has not been able to keep up pace with the requirements of the consumer electronic devices, which are increasingly becoming more diverse, functional and power hungry [3]. For personal low-power electronic devices, harvesting of energy from the mechanical movement is believed to be the most reliable route as most human activities are based on mechanical movement which is irrespective of the environment [3-5]. Recently, inorganic nanowires of ZnO, InN, GaN, CdS, ZnS and PZT have shown remarkable ability to harvest energy from small mechanical movements and have shown higher energy conversion efficiency as compared to their micro and macro sized counterparts which was attributed to size-effects, decreased defects and improved mechanical flexibility [2-10]. However, it should be noted that these materials are quite brittle in nature, work only at small levels of strain (~1%) and are much harder to integrate on a large scale and quite expensive to produce [1-5]. The criteria for wearable energy harvesting devices are that it must; (i) be imperceptible to the user; (ii) not load the user; (iii) provide long term lifetime with reasonable power densities (dependent on the application); and (iv) be cost-effective and inexpensive to produce [11]. While a number of piezoelectric device architectures, materials ($Pb[Zr_xTi_{1-x}]O_3$, $BaTiO_3$) and processes (electrospinning, lithography) have been developed to conform to the aforesaid criteria, the materials themselves are not amenable and the processes are quite tedious and expensive. Moreover, for wearable applications, the energy harvesting devices should provide the right “feel” and comfort as well to the wearer. The current problems associated with flexible piezoelectric generators are; (i) low throughput and

long and tedious processing techniques; (ii) low output power densities; and (iii) lack of integration techniques [1, 4]. Moreover, for achieving truly integrated piezoelectric materials in textile structures, the durability and the "feel" of the piezoelectric structures need to be tailored. In previously published works, the piezoelectric elements have been usually physically embedded inside a fabric by simple stitching it, or have been based on brittle PZT materials which have then been deposited by electrospinning and then transferred onto flexible substrates [5, 12]. However, PZT based materials are lead-based and hence not amenable for wearable textile applications. Recently, Wang et al have developed nanowire based generators built on textile fibres which provide electrical output via the friction motion between the fibres [13]. A device built using hydrothermally grown ZnO on PVDF fibres was shown to produce 1-2 μWcm^{-3}, however the procedure of making the device was tedious and time consuming [3]. While, electrospinning process used to produce PVDF and PVDF(TrFE) nanofibres is capable of producing flexible large area piezoelectric materials, the throughput of the process is again quite low [2, 15] and moreover the need to attach the flexible metal/metallic electrodes limits their use and lifetime. The poor fatigue resistance of the metal foil under repeated mechanical deformation leads to the failure hence making the durability a major challenge [1, 15, 16].

For energy harvesting from human movement, the fibre based electrical power generators are highly desirable as they are light weight and comfortable and look no different from the conventional fabrics. The conjunction of piezoelectric materials in fibres and therefore fabrics offers a simple route for the building of soft piezoelectric generators. The flexible textile structures can themselves be designed so as to provide piezoelectric output on low levels of strains and loadings while providing high fatigue resistance under a large number of variable mechanical deformation and loading cycles. To address this, we have used three-dimensional piezoelectric fabrics based on "3-D spacer" textile technology. The

basic definition of a three-dimensional fabric is that the Z-direction dimension is considerable relative to the X and Y dimensions [17, 18]. The thickness of the fabric or the Z dimension is maintained via the use of a spacer yarn and hence the name, 3-D spacer yarn. Thus, the spacer fabric is a three-dimensional knitted fabric consisting of two separate knitted substrates, which are joined together or kept apart by spacer yarns. The 3D spacer fabrics can be made either using warp knitted or weft knitted technologies. Warp knitted spacer fabrics are structures that consist of two separately-produced fabric layers which are joined back-to-back, wherein the spacer yarn which joins the two face fabrics joins them or spaces them apart [17, 18]. Typically, these spacer fabrics can have a thickness ranging from 1 to 15 mm, with the two faces being 0.4 to 1 mm thick. The single major feature of warp knitted spacer fabric is that virtually any thickness can be obtained (up to 65 mm reported) using suitable machines [17, 18]. The weft knitted spacer fabrics (produced in this study) can be produced on circular double jersey machines as well as electronically controlled flat machines [17, 18]. The basic structure of the spacer fabric is limited to either knitting the spacer threads on the dial and tucking on the cylinder, or tucking the spacer threads on the dial and cylinder needles [17, 18]. Also, in weft knitting, the thickness of the spacer is usually limited to between 2 and 10 mm. [17, 18] These fabrics have been studied for many years now in applications ranging from medical textiles (anti-decubitus blankets), highly breathable sportswear to foundation garments such as bra cups and industrial composites [17, 18]. However, to the best of our knowledge, the use of 3-D spacer fabrics as energy harvesting textiles has never been explored or reported.

In order to overcome the drawbacks of the existing devices and provide better energy solutions, we have explored the possibility of having highly flexible, efficient and durable piezoelectric generators based on simple processing and low-cost strategies. Here, we report our work on the development of present novel all-polymeric fibre based single 3-D structure

piezoelectric generators comprising of a PVDF monofilament spacer yarn and silver coated Polyamide 66 (PA66) yarn as the top and bottom conducting fabric faces. The generator is shown to be capable of efficiently converting mechanical energy into electrical energy; under a peak compressive pressure of 0.10 MPa, the fabric consistently produced a voltage of ~14 V and a peak current of ~30μA, corresponding to a peak power density of 5.10μWcm^{-2}, thus demonstrating a significantly higher power output under similar experimental conditions over the existing 2D woven and non-woven piezoelectric structures.

Experimental

Continuous melt-spinning extrusion of poled PVDF monofilaments

PVDF homopolymer SOLEF 1006, supplied by Solvay Solexis Ltd., was used for processing of fibres. The polymer has a melt flow index of 40g/10 min at 230^{o}C and 2.16 kg mass with the melting point and crystallisation temperatures of ~175^{o}C and 138^{o}C, respectively. The melt spinning of PVDF was carried out on a bi-component pilot plant scale extruder built by Fibre Extrusion Technology Ltd., Liverpool, United Kingdom. The polymer in pellet form is transported across the length of the heated barrel (temperature profile: 190, 200, 210, 220^{o}C, across the four heated barrel zones) via a screw, where it is compressed and gets melted through the friction generated between the granules and the high temperatures. The melt exits the monofilament spinneret (Φ=0.8 mm, 230^{o}C) at a pressure of approx. 100-105 bar where the filament is cooled down using an air quench operating at 20^{o}C. At this point the melt is taken up by a draw down godet rotating at 101 mpm (metres per minute). The filament is then passed upon two pairs of heated godets, which define the draw ratio and extension of the filament. The first of these two godets is heated upto a temperature of 80^{o}C and with a spinning speed of 102 mpm, produces a very slight draw in the filaments. The third pair of

godets produces the largest change in the orientation of the chains and the crystalline structure of the filament. These godets are rotating at 505 mpm, thereby producing a final draw ratio of 5:1 from where the filaments are finally collected on a winder running at nearly 505 mpm. The draw ratio of 5:1 was found to be the optimal value of the drawing where a high β phase (~80 %) was observed and the filament could be processed continuously without any breakages, which usually occurred above this draw ratio (*see supplementary information*). While the filaments are being drawn between the second and third pair of godets, an electric field of the order of 0.6 MV/m is applied across the filament between two metallic electrodes to further enhance the β phase of the filaments. It should be mentioned here that the β phase is not controlled during the device fabrication i.e. fabric manufacturing but rather during the melt spinning of the PVDF fibre itself. The structural properties such as the yarn diameter, tensile strength and tenacity do not in themselves control the piezoelectric properties but rather are a consequence of the drawing and poling process during the melt spinning of the fibre. The advantage of the process is that it is considerably less time consuming, since the piezoelectric fibres are poled during the fibre production process itself and can be used as such without resorting to further modifications and poling [19, 20].

Knitting of 3-D spacer piezoelectric fabrics

The fabrics were knitted on a E20 (20 needles/inch) circular weft knitting double-jersey machine with a 30" diameter at a machine speed of 30 rpm (at Baltex Speciality Knitters Ltd., Derbyshire, United Kingdom). Figure 1 illustrates the specific knitted structure produced in this work using three different yarns: (i) conductive yarn A, (ii) insulating yarn B and (iii) piezoelectric yarn C [21]. The conductive yarn A (Shieldex® Ag coated PA66, 143/34 dtex with a resistivity of <1kΩ/m, supplied by Statex GmbH), is plaited on the outside of each of the fabric face; the insulating yarn B (84 dtex, false-twist texturised polyester yarn) is plaited

inside the structure in such a manner that it shows on the inside of the two fabric faces and finally the piezoelectric monofilament spacer yarn C (300 dtex), is tucked inside the two fabric faces. In fact, the polyester insulating layer (Yarn B) has been used for two main purposes: (i) providing resilience and reinforcement to the 3-D structure and (ii) insulating the Ag coated Polyamide against the opposite face. During the initial compression test, without the insulating yarn, it was observed that beyond a certain threshold of impact (>0.02 MPa), the voltage output from the 3-D piezoelectric fabric structure was abruptly reduced to zero. On closer inspection, it was revealed that upon impact, due to the lower resilience of the structure, the PVDF spacer yarn was momentarily compressed / sheared to such an extent, that the two opposite conducting ends shorted out each other and hence no output was observed. Moreover, it was observed that the cutting of the fabric led to a lot of fraying from the loose ends of the Ag coated PA66 which could potentially connect the two opposite faces, thereby shorting it out. Thus, it was necessary to reinforce the structure as well as provide an insulating layer between the PVDF yarn and Ag coated Polyamide, so that in the cases of high impact, the integrity and the voltage output of the 3D piezoelectric textile is maintained. The two different knitted fabrics with and without the insulating yarn B are shown in Fig. 4 (*supporting information*), where the colour contrast observed is due to the addition of the insulating yarn to the structure. For compression tests, a simple experiment was designed in which a compression plate was attached to the load cell in the Instron system. The fabric sample was then connected to a voltmeter, with the voltmeter being set for measuring continuity. The compression plates were moved at a cross-head speed of 1mm/min and as soon as continuity developed across the two opposite fabric faces (*i.e.* the two opposite faces touched each other), further testing was stopped and the force required measured. It can be clearly observed from Fig. 5 (*supporting information*), that the addition of insulating yarn has reinforced the compressive load which can be sustained by the 3D piezoelectric fabric, by a

factor of 6. In fact, the compressive strength of the 3D fabric without the insulating yarn was only 0.02 MPa which was enhanced to ~0.13 MPa upon the addition of the insulating yarn (Fig. 5, supporting information). Moreover, a difference in the compression behaviour of the fabrics could be observed, where the structure without the insulating yarn provided virtually no resistance at all to the compression; whereas in the 3D structure with insulating yarn, much higher resilience was observed in terms of the load required for compression as well as the two plateaus observed in the force extension curves. This behaviour of the 3D fabrics under compression is associated with good energy adsorption capacity under compression and impact is well documented and has been reported previously as well and [17, 18]. Since, the impact pressures range applied in this work is of the order of 0.02- 0.10 MPa, which is comparable to normal human walking, clearly the fabric structures without the insulating yarn are of little use in this study and the study focuses on the development and use of 3D piezoelectric fabric structures with the insulating layer only. It should be noted that the yarn C is tucked in such a manner that it does not protrude through either of the fabric faces and always remains inside the two faces keeping them apart. The total thickness of the fabric structure made in this work is approx. 3.5 mm, however it should be noted that this thickness can be varied between 2 mm to 60 mm, depending upon the type of knitting machine used and the end application.

Characterisation

The thermo-analytical and crystalline properties of the PVDF monofilaments are characterised with differential scanning calorimetry (DSC), carried out on a TA instruments DSC Q2000, in the temperature range of -50 to 200^{o}C at a heating rate of 5^{o}C/min (under N_2 atmosphere). For DSC analysis, the specimens were prepared by rolling small amount of fibres by tweezers and placed inside the aluminium pans. Further analyses of the DSC curves

were carried out by using vendor provided Thermal Analysis software. Quantification of piezoelectric β-phase was carried out by Fourier Transformed Infra-red spectroscopy (FTIR) analysis on Thermo Scientific IS10 Nicolet FTIR spectrometer coupled with the smart iTR accessory. Vendor provided OMINIC software was used to analyse the results, including the calculation of β content. Furthermore, X-ray diffractometer (D2 Phaser, Bruker, Co Kα λ= 1.788970 Å, operating at 30 kV and 10 mA) was used to study the crystalline structure of the monofilaments. Piezoresponse Force Microscopy (PFM) measurements were carried out by using Agilent 5600LS scanning probe microscope, wherein a small section of the specimen was attached to the sample plate using silver paste. Platinum coated conductive tips (HQ: NSC14/Pt, Mikromasch) with typical resonance frequency of 160 kHz and a force constant of 5 N/m were used. A gold wire was also connected to the sample plate to apply the AC bias between the sample plate and AFM conducting tip. To ascertain a flat surface on the filament, scans were performed on an area of 10x10 μm. During the experiments, the vertical piezoresponse were recorded and PFM amplitude-phase scans were performed with AC amplitude up to 10 V and at a frequency of 10 kHz. Solid state Nuclear Magnetic Resonance (NMR) experiments were performed on a Bruker 9.4 Tesla Avance-400 wide bore spectrometer, at frequencies of 400.1 MHz (^{1}H) and 100.5 MHz (^{13}C) and magic angle spinning (MAS) rate of 12.5 kHz. Data was acquired using cross polarization (CP) MAS (^{1}H $\pi/2$ pulse length 2.5 micro-seconds, ^{1}H cross polarization field 70 kHz, ^{1}H-^{13}C cross-polarization contact time 2.5 ms, broadband two phased pulsed modulated (TPPM) decoupling during signal acquisition at a ^{1}H field strength of 100 kHz. Repetition time was 2 seconds in all experiments. ^{13}C chemical shifts were referenced to the signal of the methylene carbon of solid α-glycine at 43.1 ppm relative to tetramethylsilane at 0 ppm and the total number of scans acquired was 30k. The impact testing of the fabrics was carried out by using an Instron Dynatup 9200 test rig with the open circuit voltage being measured directly on an

oscilloscope and current with an optimal resistive load of 470 kΩ.

Results and discussion

Microstructure of poled PVDF filaments

Poly(vinylidene fluoride), PVDF, is a semi-crystalline polymer which has been widely investigated for its piezo, pyro-electric properties which are inherently related to its structure [20-25]. Upto five different crystal phases (α, β, γ, δ, ε) have been reported for PVDF out of which, α and β phases are the most common phases [20, 22]. PVDF primarily exists in the α-phase, which is thermally stable and shows a TGTG′ (T-trans, G-gauche^{+}, G′-gauche^{-}) dihedral conformation wherein the molecular dipoles are anti-parallel, resulting in non-polar crystal structure (Fig. 2(d)) [20, 22-25]. The β phase shows an all TTTT conformation wherein the polar C-F and C-H bonds possess a dipole moment perpendicular to the carbon backbone (Fig. 2(d)). Additionally, all the chains are oriented parallel to the direction of dipoles, giving β phase the highest spontaneous polarisation among all the five phases. The β phase, which is kinetically stable under ambient temperature and pressure, is the phase that exhibits outstanding piezo- and pyroelectric properties and consequently for designing of piezoelectric fabrics, is the most interesting phase [20, 22-25]. In recent years, various techniques have been used to control and enhance the formation of β phase. The polar β phase in PVDF is usually obtained by controlled crystallization from solution [26], quenching and poling of the film [27] but most frequently by uniaxial or biaxial stretching of α phase films [28]. Other techniques such as electrospinning technique [29] and more recently melt spinning under strong electric field [19, 20] have also been explored. Furthermore, the incorporation of various nanoparticles such as multiwalled carbon nanotubes [30], graphene oxide (GO) [31] or reduced graphene oxide (RGO) [32], and other polymers [33] into PVDF matrix have also been shown to influence the crystallization behaviour of PVDF.

Figure 2 (a) shows the SEM images of poled and stretched PVDF fibres, where the formation of fibril like structures, created during the stretching of the polymer chains from the melt, can be observed. The literature reports that during the melt spinning processing of PVDF filaments, the fibres are subjected to strong uniaxial drawing at high speeds which introduces a strong elongation force in the direction of draw, creating molecular orientation which leads to an increase in the crystallisation [20, 22-25]. The further drawing of the fibre enhances the mechanical properties and is accompanied by orientation of the crystallites along the fibre axis. It has been shown that with drawing, the α-phase crystallites begin to shear apart and deform into small crystallites, some of which convert into β-phase [22, 23, 33]. This transformation is associated with the transformation of the spherulitic microstructure via the "tearing-away" of small areas from the lamella and formation of micro-fibrillar structure [25, 34]. Thus, the stretching or cold drawing (below melting point) of the fibre leads to an increase in the crystallinity and consequently the strength of the fibre as ascertained by the DSC analysis *(see supporting information)*. DSC is a thermo-analytical technique often used to identify and quantify the crystalline phases of the polymers. Figure 2(b) shows the DSC curves for the starting PVDF pellets and poled melt-spun fibres; which, both of which display an endothermic peak at ~170^{o}C. However, for the poled melt-spun fibres, the endotherm is much narrower, implying a more uniform distribution of the crystalline phase as compared to the endotherm of the pellets which displays nearly two distinct melting peaks, corresponding to the presence of multiple phases. Now, the assignment of absolute melting temperature for different crystalline phases has been contentious and instead a melting range exists for the different crystalline phases [24]. According to Prest and Luca [35], the expected melting temperature, represented by the endothermal peak, of the α-phase of PVDF is 172^{o}C while Gregorio and Cestarini [36] refers that it occurs at 167^{o}C. On the other hand, β crystallites have been reported to present a

melting temperature similar to α-PVDF [37, 38] and therefore, DSC is not used often to distinguish these two phases, but to calculate the crystalline percentage of the film [24]. The degree of crystallinity (ΔXc) of each sample can be calculated according to the following equation:

$$\Delta Xc = \frac{\Delta Hm}{\Delta Hm100} \times 100\% \qquad \text{Eq. 1}$$

where ΔH_m is the melting enthalpy of the sample and ΔH_{m100} is the melting enthalpy for 100% crystalline material [24, 36-38]. For starting pellets, a low crystallinity of the order of 38.6% is observed which is enhanced to nearly 52.1% for melt spun monofilaments. In fact, the ΔXc shows a rapid increase with the increase in the draw ratio until the draw ratio of 5:1, beyond which it starts to reduce *(see supporting information for detailed discussion)*. Similar results have been reported by various groups such as Lund et al, Gregorio et al and Gomes et al among others [22-25, 33, 34].

The FTIR spectrum of melt-spun filament and the starting pellets is shown in Figure 2(c). It can be clearly observed that the starting pellets consist of primarily α-phase, as evident by the strong characteristic absorbance bands at 760, 796 and 974 cm^{-1} [25, 37-40]. For poled melt-spun fibres, the emergence of peaks at 840, 1276 and 1430 cm^{-1} corresponding to the β phase can be clearly observed, along with a corresponding decrease in the peak at 760 cm^{-1} [37-40]. Furthermore, this change in the β-phase can be quantified using the following equation:

$$F\beta = \frac{X\beta}{X\alpha + X\beta} = \frac{A\beta}{A\beta + 1.26A\alpha} \qquad \text{Eq. 2}$$

where A_α and A_β are their absorption bands at 760 and 840 cm^{-1} [25, 37-40]. Using the above equation, the β-phase content for pellets is calculated to be ~39.1 % and for poled melt-spun fibres the value is nearly 80%. Similar results have been observed by various authors where it was shown that both the stretching temperatures (80-100^oC range) as well as the drawing

ratios have a detrimental effect on the β-phase content [25, 37-40]. It has been suggested by Lund et al., that an increase in the drawing ratio leads to a higher conversion from the α-phase to β-phase with a strong correlation between the drawing speeds and the conversion between the phases [22, 41]. During melt extrusion of PVDF monofilaments, the filaments are subjected to uniaxial drawing at moderate to high rates, depending upon the take-off speed on the winder [22, 33, 41]. This uniaxial drawing introduces a strong axial flow creating molecular orientation along the drawing direction, leading to an increase in crystallisation [22, 33, 41]. This crystallisation also changes the morphology of the structure from spherulitic (predominantly α phase and at low drawing ratios) to more fibril like (predominantly β phase and at high drawing ratios done at high speeds (~500 mpm) [22, 33]. Also, the presence of the applied electric field further promotes the formation, alignment and locking-in of the β-phase and is discussed further in the later sections. The X-ray diffractograms obtained for PVDF pellets and poled melt-spun fibres are shown in Fig. 2(d)**.** The results show that the melt spinning followed by drawing has a profound effect on the formation of β phase in the monofilaments. In the XRD scan of starting PVDF pellets, a peak at ~ 21.3^{o}, corresponding to a sum of diffractions from the (100) and (020) planes is observed along with another diffraction peak at 23.1^{o} corresponding to (110) plane [20, 24, 42, 43]. The diffraction from (021) plane leads to the appearance of peak at 30.9^{o}. All these three peaks can be characterised to α phase of PVDF **[**20, 24, 42, 43**].** Upon the melt spinning process, only one peak at 24^{o} can be observed, which peak refers to the sum of (200) and (110) β-phase diffraction planes and may include diffractions from residual (110) α planes [20, 24, 42, 43]. The broadening of the peak attributed to the β-phase can be attributed to multiple factors such as small crystallite size and defects in crystalline lattice due to occurrence of unit cells with deviating dimension [22]. During melt spinning at high draw ratios and fast godet speeds, the phase transformation occurs via the deformation of α-

crystallites into smaller crystallites which are then converted to β-phase and hence the broadening of the peak can be largely ascribed to the small crystallite size. The presence of a small shoulder is also observed at 21.5^{o}, which can be attributed to the residual α content present. These results are in agreement with the FTIR and DSC results where the formation of β phase was confirmed along with the presence of some residual α phase.

As mentioned earlier, the presence of applied electric field (poling) during drawing promotes the formation and locking in of the β-phase domains. The ^{13}C NMR spectroscopy of PVDF has not been extensively reported and from the existing solution-state ^{13}C NMR, the $–CH_2$ and $–CF_2$ of the main chain have been identified along with the low-intensity signals which have been ascribed to $–CF_2$ and $–CH_2$ in defect units. The difference in the $–CH_2$ carbon shifts of α and β phases has been observed in solid-state NMR by filtration of the amorphous phase using a post CP T_{1p} filter, where α and β phases give rise to signals at 43.0 and 42.1 ppm. Figures 2(e) to 2(g) show the ^{13}C-NMR result of the poled and unpoled melt-spun PVDF fibres. Since, both of the samples have same draw ratios and similar β phase values (see supporting information), there should no be any variation in the $–CH_2$ and $–CF_2$ NMR shifts. However, significant changes in the line shape and line width of the $–CF_2$ (~122 ppm) and specifically the $–CH_2$ carbon (~44 ppm) are observed after the poling of the fibre. Both these bands show sharpening after poling which can be attributed to a change in the distribution of the backbone torsion angles, which tend to alter under the applied electric field present during the poling process [44-46]. As a consequence, the proportion of cis:trans conformation around the atomic microenvironments is changed and hence the distribution of chemical shifts changes in the polymeric backbone. In addition to the main resonance lines of CH_2 and CF_2, further low intensity signals are observed in the range of 26 ppm. These shifts can be interpreted as arising from head-to-head or tail-to-tail sequences in the chain and occur due to the presence of defects in the structure which can be as high as 5-6%. Thus, the

simultaneous drawing and the application of electric field helps in the formation of β phase wherein the distribution of $–CF_2$ and $–CH_2$ is altered further leading to a possible enhancement in the β phase [44-46].

Piezoelectric effects in PVDF filaments and 3-D spacer textiles

Now, it is of particular importance to determine the piezoelectric constant d_{33}, the induced polarization per unit stress applied in the out-of-plane (poling) direction. Piezoresponse force microscopy (PFM) has become the accepted method for quantifying d_{33} where small displacements are involved [47-49] For PFM, an alternating current signal is first applied between a conducting atomic force microscope (AFM) tip (usually Pt) and a bottom contact electrode after which the conducting tip is brought into contact with the surface. The electromechanical response of the sample is detected as the deflection of the tip that simultaneously supplies simultaneously applies ac bias and detects vertical electromechanical response through tip deflection. The ac amplitude was ramped from 0 to 9V and effective piezoelectric coefficient was calculated from linear fit between displacement and the ac bias amplitude. The piezoelectric constant d_{33} at any given point can be described by the following equation:

$$\vartheta = \delta A d_{33} \qquad \text{Eq. 3}$$

where ϑ is the amplitude of the piezoresponse signal, A is the amplitude of the testing AC voltage and δ is the conversion factor between the mechanical displacement of the PFM tip and the electrical deflection signal [49]. Figure 7(a-d) shows the acquired topography and piezoelectric amplitude images of the obtained of poled and unpoled melt-spun fibres (drawn at the same draw ratio). It can be clearly observed that poled melt-spun fiber shows higher Piezoresponse and using the equation shown of with an effective d_{33} value of nearly 17.1 pm/V as compared to 7.68 pm/V obtained for the unpoled melt-spun fiber. Now, the results

from the FTIR analysis show that the β phase for both the poled and the unpoled samples is quite similar to each other and hence, there should not be any major differences between the d_{33} values for the samples (*see supporting information*). However, the d_{33} value of the poled sample is nearly twice that of the unpoled sample. It can be argued that while the initial drawing of the monofilament provides the orientation of the crystallites in the direction of the drawing, the dipole formation via the re-orientation of the $-CF_2$ groups occurs during the application of the electric field only. This assumption is supported by the NMR analysis where a change in the proportion of the cis:trans conformation around the polymeric backbone was observed upon the application of electric field.

As mentioned earlier, until now the only way to integrate piezoelectric component into the textiles was to actually embed the commercial PVDF film based sensors inside the textiles by stitching them together or through nonwoven PVDF fabrics made by electrospinning or by transferring the brittle nanowires onto a flexible substrate which is further integrated to the textile structure [1, 5, 12]. However, for true integration to occur, the textiles themselves should become the active component and not just act as a matrix to hold the active component in place. While, a few attempts have been made to make simple 2-D textile structures using piezoelectric and conductive yarns, the use of nonwoven or electrospun fabrics makes the process difficult to scale up [1, 2, 4, 14]. Moreover, the 2D textile structures are prone to fatigue and on extended use over time the textile structures will fail [17, 50]. For the all fibre piezoelectric generator produced in this work, with an effective area of 15 cm x 5.3 cm, the peak values of the open-circuit voltage and current were found to be 14 V and 29.8 μA, respectively at an applied pressure of 0.106 MPa. In fact, the total power output increases from 0.08 mW to 0.4 mW over the measured impact range of 0.02 MPa to 0.106 MPa, as shown in Figs. 4(a) to 4(c). The power output of the piezoelectric fabric can be modelled by using the following equation:

$$Power\ output = 4.98 - \frac{5.10}{(1+\exp\ (x-0.03/0.008))} \qquad \text{Eq. 4}$$

where x is the applied impact pressure and power output is measured in μWcm^{-2}. The 3D structures provide nearly five times the output power density, with a maximum power density of 5.07 μWcm^{-2} (vs. 1.18 μWcm^{-2} for knitted 2D structures, *see supporting information*). The power densities from 3D piezofabric are much higher than those reported for 2D nonwoven $NaNbO_3$-PVDF nanofibre based generators which provide a power output of 2.15 μWcm^{-2} (corresponding to an output of 3.4 V and 4.48 μA, at impact pressures of 0.2 MPa) [1] and electrospun nonwoven PVDF fabrics which generated nearly 3.2 μWcm^{-2} (corresponding to 2.05 V and 3.12 μA at impact pressures of 0.05 MPa) [2]. These values are also significantly higher than 0.43 V and 0.78 μA achieved by PVDF nanofibre based generators and 3.2 V and 72 nA achieved by $NaNbO_3$ nanowires in PDMS envelope, which provide an effective power output of 0.115 μWcm^{-2} [16]. The excellent performance of our novel generator can be attributed to the following factors: (i) high β phase of the PVDF fibres, (ii) enhanced charge collection due to intimate contact between the PVDF fibres and conductive yarns leading to improved efficiency and (iii) transfer of the uniform compression pressure across the fabric surface. The 3D structure of the fabric makes it quite "porous" in nature and hence relatively easy to compress. When the structure is impacted, then the direction of the applied force and the direction of the produced dipoles is the same, hence making the active mode as d_{33} (transverse mode). Due to the largely insulating nature of the PVDF fibres, the generated charges are separated at the opposite faces resulting in a potential difference across the thickness of the fabric structure [1]. Furthermore, these energy harvesting textiles can be coupled up with the knitted and screen printed carbon-fibre based supercapacitors for energy storage in wearable electronics which opens up a completely new field of textile based energy harvesting and storage [51, 52].

In order to test the performance of the nanogenerators, mechanical input induced electrical outputs are often measured for a large number of nanofibres of the piezoelectric material [4, 53, 54]. These signals are often very small (mV voltage output and nA-μA current range) and are difficult to measure due to the nature of the small size of the nanofibers. It is especially problematic when dealing with single nanofiber structures such as ZnO based nanogenerators [4, 53, 54]. For example, the capacitance changes between the wires and the electrodes and possible electrical coupling of the measurement instruments could surpass the real nanofiber signals [4, 53, 54]. Therefore, it is important to filter out or reject noises generated from the surrounding experimental environment. Some of these experimental validation conditions have been previously proposed for semiconductor-based or ceramic-based nanogenerators such as ZnO nanowires including Schottky behaviour, switching polarity and superposition test; for PVDF nanogenerators, the Schottky behaviour test does not apply [4]. For 3D piezoelectric fabrics, upon reversing the electrode connections, a switching in the polarity of the observed signal was observed, demonstrating that the output signal is indeed from the 3D piezoelectric fabric only rather than instrumental noise or any other artefact (see fig. 6, supporting information). To observe the superposition phenomena, both the samples need to be impacted simultaneously. To this effect, instead of using two large sample sizes (15 x 5.3 cm), the samples were cut into smaller sizes of approx. 5 cm x 6 cm to accommodate under the impact tester with an applied impact pressure of ~0.02 MPa. During the impact tests, the samples were impacted simultaneously in different configurations where (a) the output of the two samples would add up and (b) the output of the two samples would cancel out each other. In the condition where the sample output added up together a voltage of nearly 8 V was obtained (each of the samples on individual tests showed a voltage output of nearly 4.3 V each at same applied impact pressures). In the case when the samples were such connected

that they would cancel out the voltage output of each other a voltage of nearly 1 V was observed as shown in Fig. 7 (supporting information)

Now, the technologies for knitting of 3D spacer fabrics have been around for over three decades now [17, 18] and the underlying technology and understanding is highly developed. However, we understand that there have been no previous reports on the use of 3D spacer fabrics as energy harvesting fabrics and as is the case with every technological development, there are some foreseeable technical challenges which include: (i) optimisation of positioning, spacing and the thickness of the spacer piezoelectric yarn and its arrangement in the 3D structure to enhance the piezoelectric response; (ii) optimisation of fabric density, thickness of the spacer fabric for different applications, (iii) ensuring that the conducting yarns used in the opposite faces do not come in contact with each other during the knitting process or during the cutting procedure, (iv) as the textiles are intended for use as wearable energy harvesting textiles, the important factors such as air permeability, wicking properties, stretchability and recovery need to tested and controlled to provide high level of comfort to the user, and finally (v) the effects of wear and tear, washing and regular use also need to be verified to ensure reproducibility of the piezoelectric response and provide a certain lifetime value for the fabric. Especially, the conductivity of the Ag coated PA66 yarn, which is responsible for charge transfer across the faces of the fabric needs to be monitored carefully over the lifetime of the 3D piezoelectric fabric. The measurements of the electrical output as a function of number of impact cycles (~ 150 cycles, see Fig. 8, supporting information) was conducted to comment on the stability of these 3D piezoelectric fabrics. It can be clearly observed that the electrical output shows very little variation of 9.93 ± 0.47V in the time duration tested. Thus, the 3D piezoelectric fabrics can provide an efficient and novel way to overcome the stability issues presented by the poor fatigue resistance of the metallic electrodes [1, 15, 16, 55]. Further tests are being carried out to assess the long-term stability

and durability of the fabrics and will be the subject of a separate study. Further work on the coupled mechanical and piezoelectric analysis of the 3-D fabric generators is under way to ascertain the complex relationship between the structure of the fabric and power output and to enhance it further.

Conclusions

In summary, a novel all fibre piezoelectric nanogenerator comprising of principally β-phase PVDF fibres in a three dimensional spacer structure, with Ag coated Polyamide yarn as the charge collecting conducting faces, has been designed, developed and fully characterised. The phase change from a predominantly α phase in raw pellets to nearly 80% β-phase in filaments has been obtained by drawing of the fibre under an applied electric field. The α to β phase transition has been quantified by using a variety of techniques including FTIR, DSC, NMR, XRD and PFM analysis where it was observed that the application of electric field has a profound effect on the rotation of the $–CF_2$ and $–CH_2$ groups responsible for the introduction of the piezoelectric phase in PVDF. The 3D spacer piezoelectric fabrics exhibits power density in the range of 1.10 μWcm^{-2} to 5.10 μWcm^{-2} at applied impact pressures of 0.02 MPa to 0.10 MPa. This all fibre piezoelectric fabric possesses the advantage of efficient charge collection due to intimate contact of electrodes and uniform distribution of pressure on the fabric surface, leading to enhanced performance. Also, the fabric can be cut into any shape and size without compromising on its flexibility and offers a simple route to integration. Moreover, the “feel” of the all-fibre piezoelectric generator is not very different from any other conventional textile material and is soft and flexible providing potential maximum level of comfort to the wearer. Bearing all these merits in mind, we believe our method of producing large quantities of high quality piezoelectric yarn and piezoelectric fabric provides an effective option for the development of high performance energy-

harvesting textile structures for electronic devices that could be charged from ambient environment or by human movement.

Author contributions

N.S. designed the experiments with the initial discussion with T.H.S., S.C.A., J.G. and E.S.. The textile structure was designed by S.C.A. along with T.H.S and N.S. The monofilaments were prepared by N.S. along with W.P. with technical input and direction from R.L.H. and D.V.B.. The PFM experiments were performed by P.M. and N.S.. The XRD data was collected by S.S. and N.S.. The NMR data was collected by D.G.R. and J.G.. The final manuscript was prepared by N.S. and all the authors discussed the results.

Figure Captions:

Fig. 1 (a) Schematic of fabric structure with the position of various yarns in the structure, (b) cross-sectional SEM image of the actual fabric clearly showing the position of piezoelectric and conductive yarns

Fig. 2 (a) SEM images of the poled and drawn fibre, (b) DSC scans of the starting PVDF pellets and the prepared fibres showing the stark change in the melting endotherms, (c) enhancement of vibration associated with β phase measured with FTIR, (d) XRD spectra of pellets and fibres showing the enhancement of the β phase , (e-g) NMR data showing the change in the peak shapes of $–CH_2$ and $–CF_2$ signals for poled melt-spun and unpoled melt-spun fibres, the torsion angles φ1 is $-CF_2$ centred and φ2 is $-CH_2$ centred

Fig. 3 Simultaneously obtained PFM topography of (a) poled melt-spun fibre and (d) unpoled melt-spun fibre (the red arrow shows the stretching direction); PFM phase of (b) poled melt-spun fibre and (e) unpoled melt-spun fibre; and PFM amplitude of (e) poled melt-spun fibre and (f) unpoled melt-spun fibre

Fig. 4 (a) Schematic structure of the packaged 3D piezoelectric fabric power generator; typical (b) voltage and (c) current outputs of the 3D piezoelectric fabric (obtained at impact

pressure of 0.034 MPa across a 470 kΩ load), (d) variation of total output power as a function of applied impact pressure for 2D and 3D piezoelectric fabrics.

Acknowledgements

The research was supported by the Northwest Regional Development Agency through the Knowledge Centre for Materials Chemistry.

References:

[1] W. Zeng, X. Tao, S. Chen, S. Shang, H. L. W. Chan, A. S. Choy, *Energy Environ. Sci.* **2013**, 6, 2631

[2] J. Fang, H. Niu, H. Wang, X. Wang, T. Lin, *Energy Environ. Sci.* **2013**, **6**, 2196

[3] M. Lee, C. Y. Chen, S. Wang, S. N. Cha, Y. J. Park, J. M. Kim, Z. L. Wang, *Adv. Mater.* **2012**, 24(13), 1759

[4] J. Chang, M. Dommer, C. Chang, L. Lin, *Nano Energy* **2012**, *1*(3), 356

[5] W. Wu, S. Bai, M. Yuan, Y. Qin, Z. L. Wang, T. Jing, *ACS Nano* **2012**, *6*(7), 6231

[6] Z. L. Wang, J. Song, *Science*, **2006**, 312, 243

[7] Y. F. Lin, J. H. Song, Y. Ding, S. Y. Lu, Z. L. Wang, *Adv. Mater.* **2008**, 20, 3127

[8] M. Y. Lu, J. H. Song, M. P. Lu, C. Y. Lee, L. J. Chen, Z. L. Wang, ACS Nano **2009**, 3, 357

[9] C. T. Huang, J. H. Song, C. M. Tsai, W. F. Lee, D. H. Lien, Z. Y. Gao, Y. Hao, L. J. Chen, Z. L. Wang, *Adv. Mater.***2010**, 22, 4008

[10] R. Yang, Y. Qin, L. Dai and Z. L. Wang, *Nat. Nanotechnol.***2009**, 4, 34

[11] P. D. Mitcheson, E. M. Yeatman, G. K. Rao, A. S. Holmes, T. C. Green, *Proceedings of the IEEE*, **2008**, *96*(9), 1457

[12] J. Granstrom, J. Feenstra, H. A. Sodano, K. Farinholt, *Smart Mater. Struct.* **2007**, 16 1810

[13] Y. Qin, X. D. Wang, Z. L. Wang, *Nature* **2008**, 451, 809

[14] D. Mandal, S. Yoon, K. J. Kim, *Macromol. Rapid Commun.* **2011**, *32*(11), 831

[15] S. Cha, S. M. Kim, H. Kim, J. Ku, J. I. Sohn, Y. J. Park, B. G. Song, M. H. Jung, E. K. Lee, B. L. Choi, J. J. Park, Z. L. Wang, J. M. Kim, K. Kim, *Nano Lett.* **2011**, 11, 5142

[16] J. Fang, X. G. Wang, T. Lin, *J. Mater. Chem.* **2011**, 21, 11088

[17] J. Yip, S. P. Ng, *J. Mater. Process. Technol.*, **2008**, 206(1), 359

[18] X. Hou, H. Hu, V. V. Silberschmidt, *J. Mater. Sci.*, **2012**, 47(9) 3989

[19] E. Siores, R. L. Hadimani, D. Vatansever, **2012**, WO Patent WO/2012/035350,

[20] R. L. Hadimani, D. V. Bayramol, N. Soin, T. Shah, L. Qian, S. Shi, E. Siores, *Smart Mater. Struct.* **2013**, *22*(7), 075017

[21] U.K. Patent applied for, application no. 1313911.8, N. Soin, T. H. Shah, S. C. Anand, E. Siores, University of Bolton

[22] A. Lund, B. Hagström, *J. Appl. Polym. Sci.* **2010,** *116*(5), 2685

[23] W. Steinmann, S. Walter, G. Seide, T. Gries, G. Roth, M. Schubnell, *J. Appl. Polym. Sci.* **2011**, *120*(1), 21-35.

[24] P. Martins, A. C. Lopes, S. Lanceros-Mendez, *Prog. Polym. Sci.* **2013,** http://dx.doi.org/10.1016/j.progpolymsci.2013.07.006

[25] A. Ferreira, P. Costa, H. Carvalho, J. M. Nobrega, V. Sencadas, S. Lanceros-Mendez, *J. Polym. Res.***2011**, *18*(6), 1653

[26] G. J. Rinaldo, S. B. Daniel *Polymer*, **2009**, 49(18):4009–4016

[27] L. L. Sun, B. Li, Z. G. Zhang, W. H. Zhong, *Eur Polym J.*, **2010**, 46(11):2112–2119

[28] P. Sajkiewicz, A. Wasiak, Z. Goclowski, *Eur Polym J*., **1999**, 35(3): 423–429

[29] J. S. Andrew, D. R. Clarke, *Langmuir*, **2008**, 24(3):670–672

[30] L. H. He, X. Qun, C. W. Hua, R. Song, *Polym Compos.*, **2010**, 31(5):921–927

[31] R. Song, D. B. Yang, L. H. He, *J Mater Sci* **2007**, 42(20):8408–8417

[32] D. Shah, P. Maiti, E. Gunn, D. F. Schmidt, D. D. Jiang, *Adv Mater.*, **2004**, 16(14):1173 1177

[33] A. Ziabicki, **1976,** Fundamentals of Fibre Formation; Wiley: Bath, England

[34] J. Gomes, J. S. Nunes, V. Sencadas, S. Lanceros-Mendez, *Smart Mater. Struct.* **2010**, *19*(6), 065010

[35] W. M. Prest, D. J. Luca, *J. Appl. Phys.* **1978,** 49, 5042

[36] R. Gregorio, M. Cestari, *J. Polym. Sci. B: Polym. Phys.* **1994**, 32, 859

[37] R. Imamura, A. B. Silva, R. Gregorio Jr, *J. Apply. Polym. Sci.* **2008,** 110, 3242

[38] S. Lanceros-Méndez, J. F. Mano, A. M. Costa, V. H. Schmidt, *J. Macromol. Sci: Phys.* **2001**, B40, 517

[39] A. Salimi, A. A. Yousefi, *Polym. Test.* **2003**, 22, 699

[40] A. B. Silva, C. Wisniewski, J. V. A. Esteves, R. Gregorio, *Ferroelectrics,* **2011**, 413, 1, 220

[41] K. Katayama, T. Amano, K. Nakamura, *K. Kolloid-Z Z Polym.* **1967**, 226, 125

[42] M. C. Branciforti, V. Sencadas, S. Lanceros-Mendez, J. R. Gregorio, *J. Polym. Sci. B: Polym. Phys.* **2007**, 45, 2793

[43] J. R. Gregorio, *J. Appl. Polym. Sci.* **2006**, 100, 3272

[44] T. Montina, P. Wormald, P. Hazendonk, *Macromolecules* **2012**, 45, 6002-6007

[45] C. Hucher, F. Beaume, R. P. Eustache, P. Tekely, *Macromolecules* **2005**, 38, 1789-1796

[46] P. Holstein, U. Scheler, R. K. Harris, *Magn. Reson. Chem.* **1997**, 35, 647-649

[47] S. V. Kalinin, D. A. Bonnell, *Phys. Rev. B.* **2002**, *65*(12), 125408

[48] M. H. Zhao, Z. L. Wang, S. X. Mao, *Nano Lett.* **2004**, *4*(4), 587

[49] C. Harnagea, A. Pignolet, M. Alexe, D. Hesse, U. Gösele, *Appl. Phys. A*, **2000**, *70*(3), 261

[50] A. P. Mouritz, M. K. Bannister, P. J. Falzon, K. H. Leong, *Composites Part A **1999**, 30*(12), 1445

[51] K. A. Jost, D. Stenger, C. R. Perez, J. McDonough, K. Lian, Y. Gogotsi, G. Dion, ***Energy Environ. Sci.***, **2013**, **6**, 2698-2705.

[52] K. A. Jost, C. R. Perez, J. K. McDonough, V. Presser, M. Heon, G. Dion, Y. Gogotsi, *Energy Environ. Sci.*, **2011**, 4(12), 5060-5067.

[53] R. Yang, Y. Qin, C. Li, L. Dai, Z. L. Wang, *Appl. Phys. Lett.* **2009**, 94, 022905

[54] A. Koka, Z. Zhou, H. A. Sodano, ***Energy Environ. Sci.***, **2014**,**7**, 288-296

[55] D. Vatansever, R. L. Hadimani, T. Shah, E. Siores, *Smart Mater. Struct.*, **2011**, 20 (5), 055019

Figures

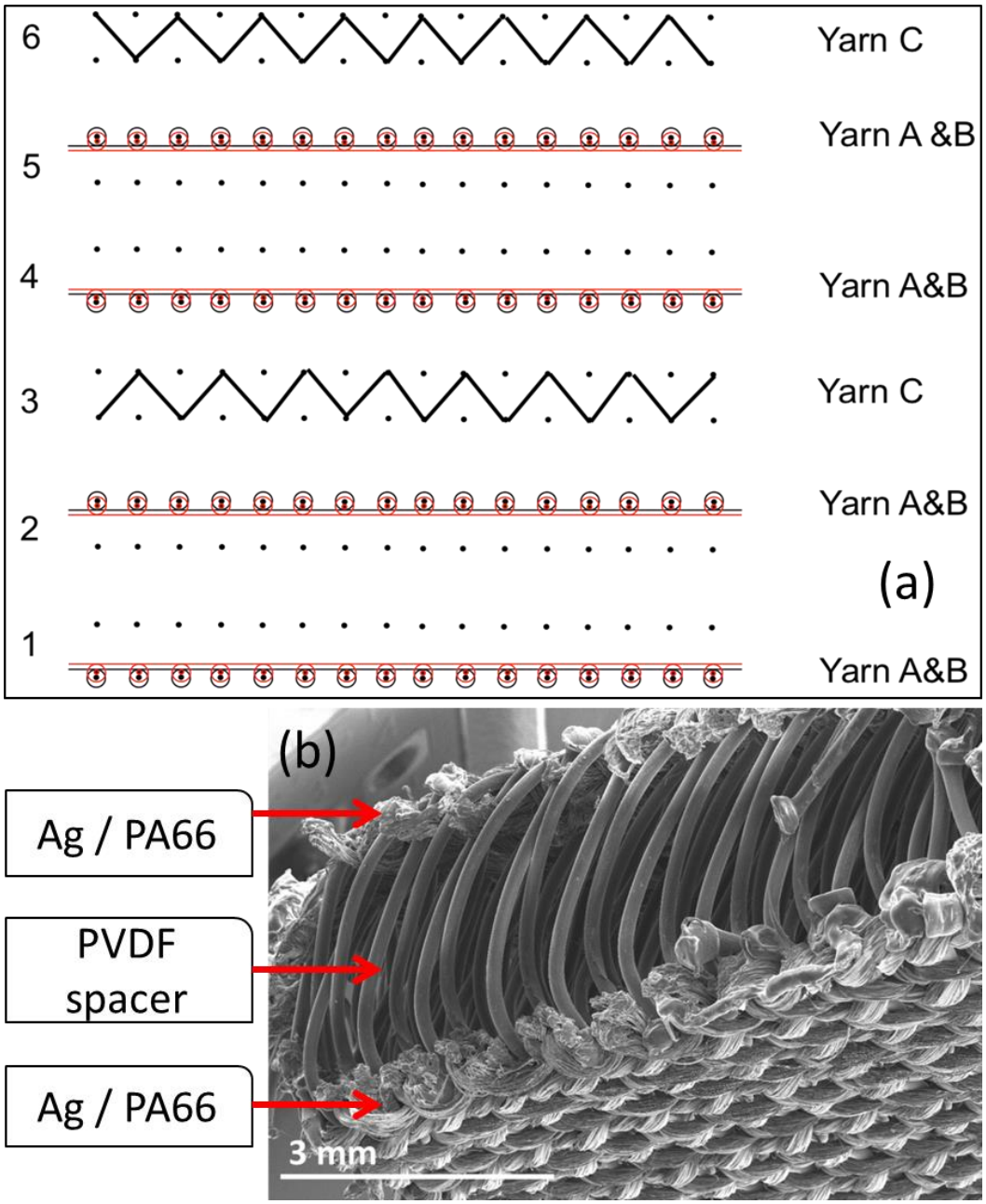

Fig. 1 of 4

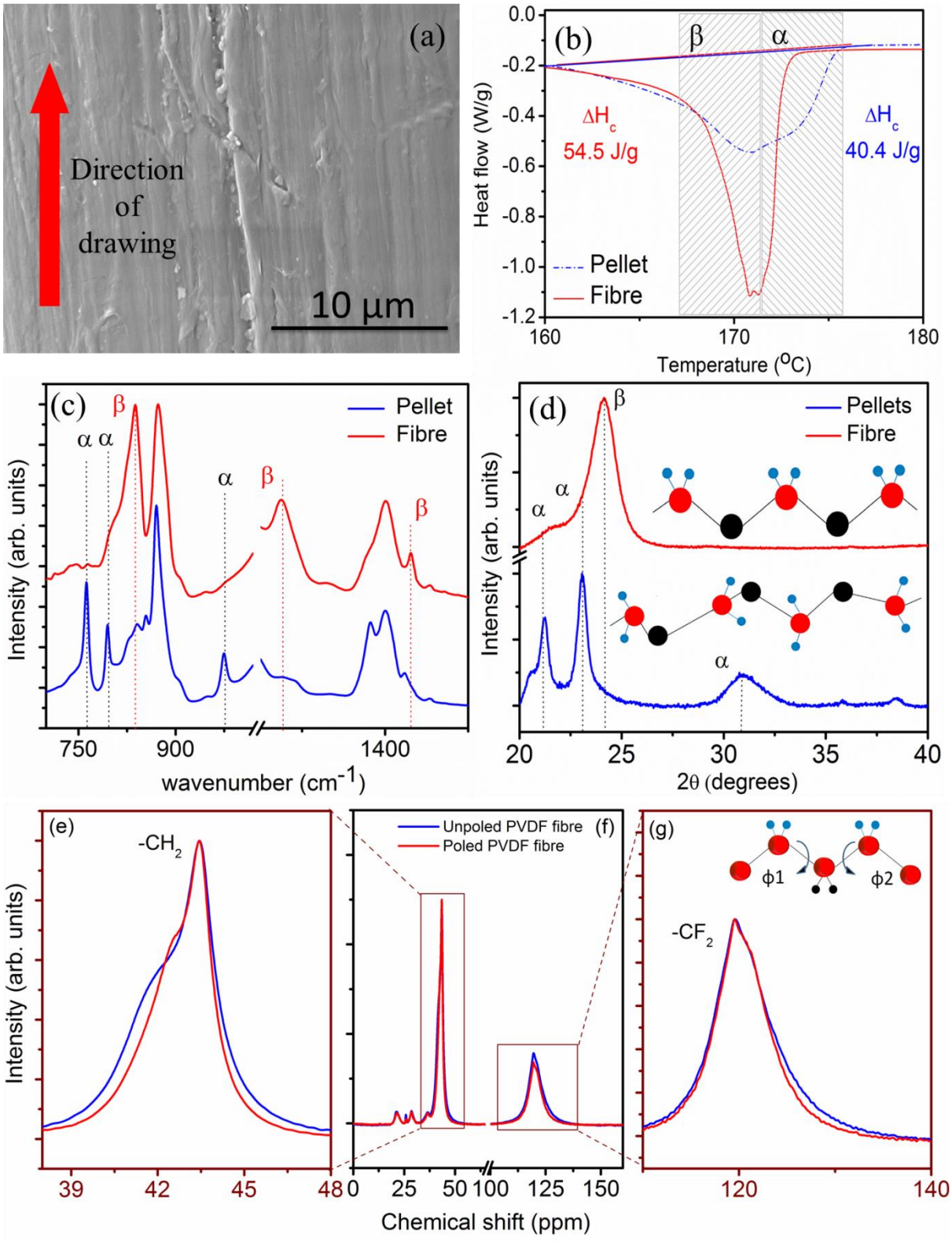
(a)
Direction of drawing
10 µm
(b)
β
α
ΔH_c
54.5 J/g
ΔH_c
40.4 J/g
Heat flow (W/g)
Pellet
Fibre
Temperature (°C)
(c)
Pellet
Fibre
Intensity (arb. units)
wavenumber (cm^-1)
(d)
Pellets
Fibre
Intensity (arb. units)
2θ (degrees)
(e)
-CH2
Intensity (arb. units)
(f)
Unpoled PVDF fibre
Poled PVDF fibre
Chemical shift (ppm)
(g)
ϕ1
ϕ2
-CF2

Fig. 2 of 4

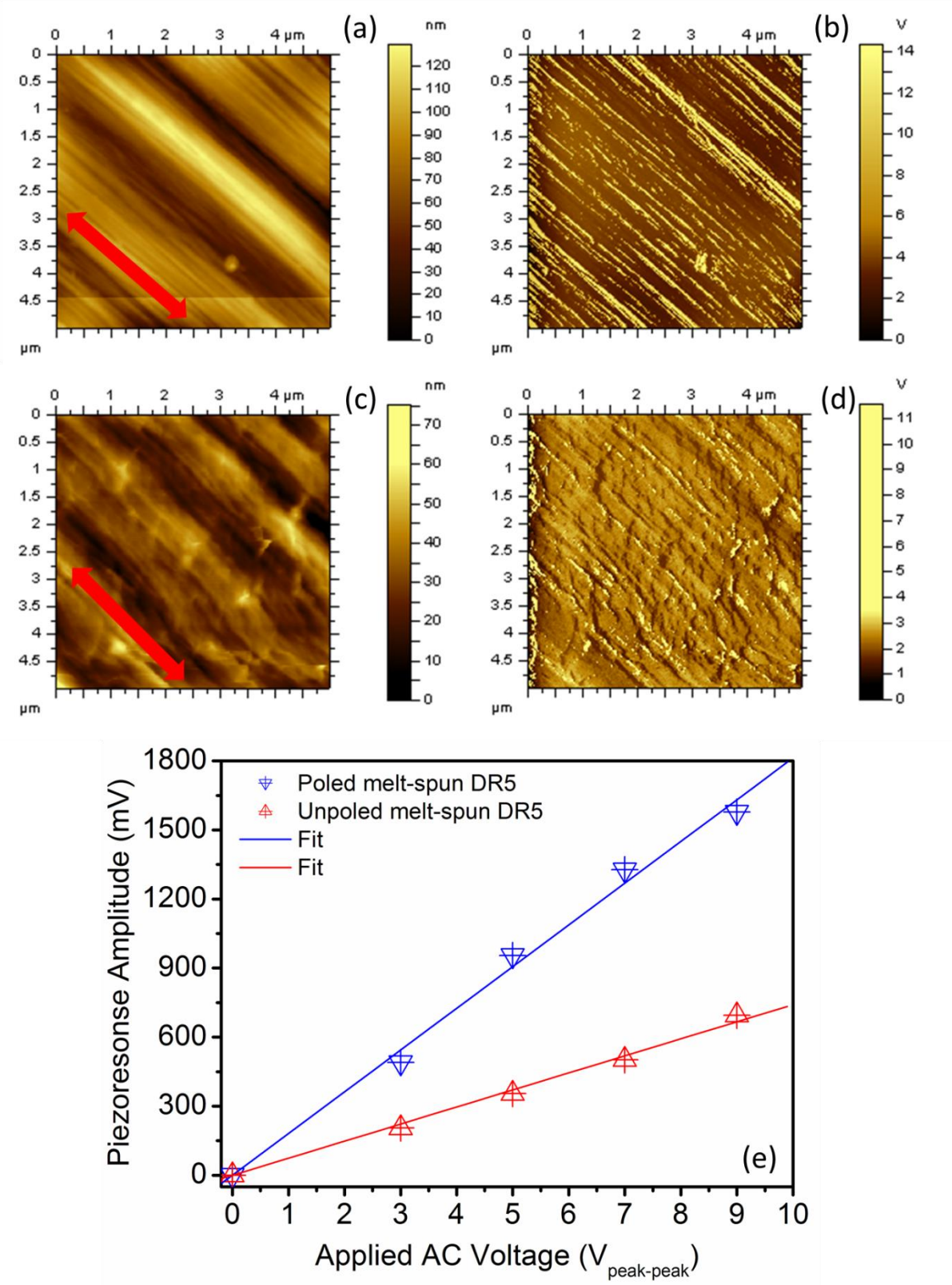
(a)
(b)
(c)
(d)
(e)
nm
V
μm
Poled melt-spun DR5
Unpoled melt-spun DR5
Fit
Fit
Piezoresonse Amplitude (mV)
Applied AC Voltage (V peak-peak)

Fig. 3 of 4

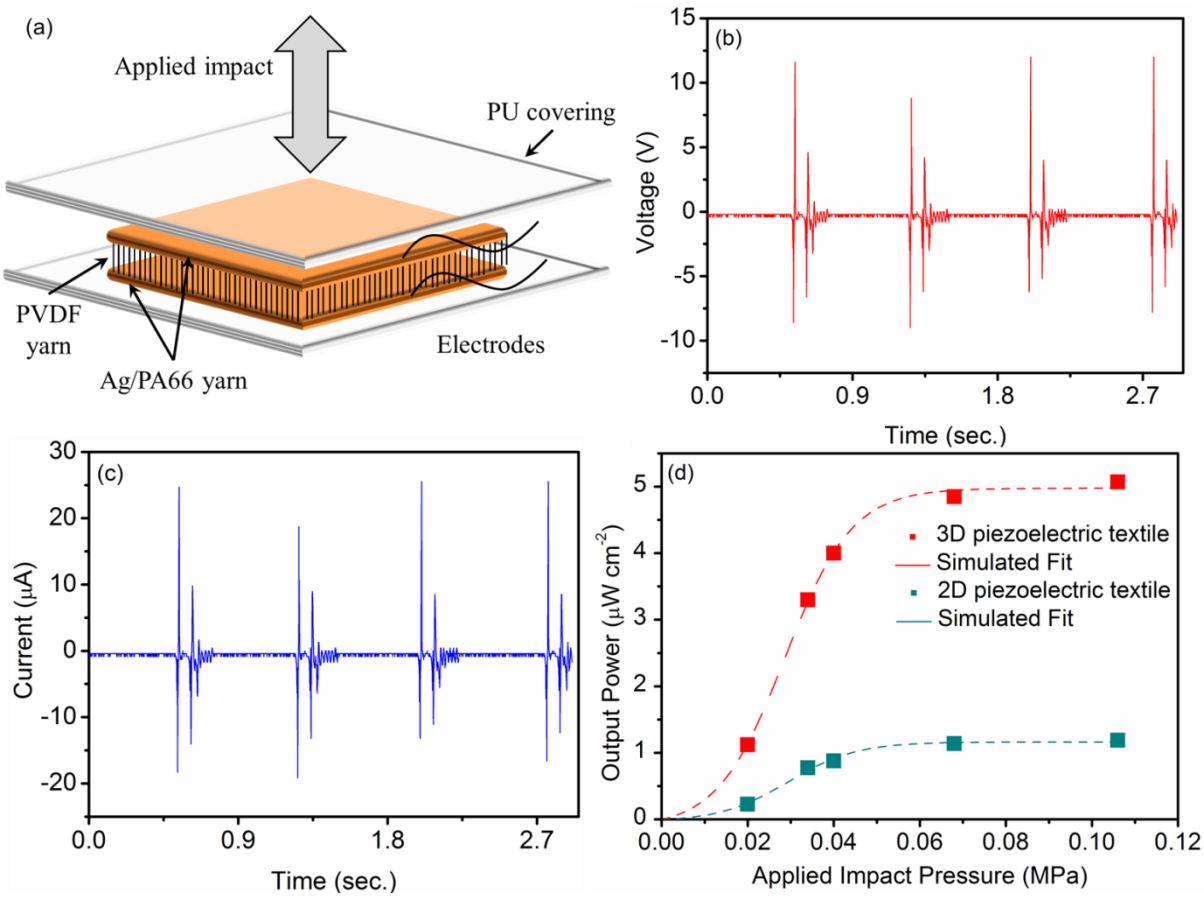
(a)
Applied impact
PU covering
PVDF
yarn
Ag/PA66 yarn
Electrodes
(b)
Voltage (V)
Time (sec.)
(c)
Current (μA)
Time (sec.)
(d)
Output Power (μW cm-2)
Applied Impact Pressure (MPa)
3D piezoelectric textile
Simulated Fit
2D piezoelectric textile
Simulated Fit

Fig. 4 of 4

Supporting information

Energy harvesting textiles: novel "3-D spacer" all fibre piezoelectric textiles

Navneet Soin,[a] Tahir H. Shah,[a] Subhash C. Anand,[a] Junfeng Geng,[a] Wiwat Pornwannachai,[a] Pranab Mandal,[b] David Reid,[c] Surbhi Sharma,[d] Ravi L. Hadimani,[e] Derman Vatansever Bayramol,[f] and Elias Siores[a]*

[a]Institute for Materials Research and Innovation (IMRI), Knowledge Centre for Materials Chemistry (KCMC), University of Bolton, Deane Road, BL3 5AB, United Kingdom

[b]Department of Chemistry, University of Liverpool, Liverpool L69 7ZD, Merseyside, United Kingdom

[c]Department of Chemistry, University of Cambridge, Cambridge, CB2 1EW, United Kingdom

[d]Department of Chemical Engineering, University of Birmingham, Edgbaston, Birmingham, B15 2TT, United Kingdom

[e]Department of Electrical and Computer Engineering, Iowa State University, Ames, Iowa 50011, United States of America

[f]Department of Textile Engineering, Namik Kemal University, Corlu-Tekirdag, 59860, Turkey

* Author Email Address n.soin@bolton.ac.uk

Institute of Materials Research and Innovation (IMRI), Knowledge Centre for Materials Chemistry (KCMC), University of Bolton, Bolton, Deane Road, BL3 5AB, United Kingdom

Telephone +44(0) 1204903118

1. **FTIR analysis of PVDF fibres at different draw ratios:**

The FTIR spectrum of monofilaments drawn and poled at different ratios is shown in figure 1(a). It can be clearly observed that the free-fall fibres (unpoled and undrawn fibres at a draw ratio of 1:1) consist of primarily α-phase, as evident by the strong characteristic absorbance bands at 760, 796 and 974 cm^{-1} [1, 2]. Previous reports from literature have reported that the uniaxial stretching of PVDF films and fibres results in the appearance of β phase [1, 2]. From figure 1(a), it can be observed that upon drawing in the presence of electric field, the formation of β phase is promoted. The peaks at 840, 1276 and 1430 cm^{-1} corresponding to the β phase can clearly be observed with an increase in the drawing ratio, with a corresponding decrease in the peak at 760 cm^{-1}, corresponding to the α-phase [1,2]. Furthermore, the β phase for all the samples can be calculated using the following equation:

$$F_\beta = \frac{X_\beta}{X_\alpha + X_\beta} = \frac{A_\beta}{1.26A_\alpha + A_\beta}$$

where X_α, X_β are crystalline mass fractions of α and β phase and the A_α and A_β are their absorption bands at 760 and 840 cm^{-1} [1, 2]. Using the equation shown above, the calculated β content for unpoled undrawn fibres is approx. 39.1 % and for drawn and poled samples increases rapidly (upto a draw ratio of 5) as a function of the drawing rate to reach nearly 78.9 %. Beyond the draw ratio of 5:1, the increase in the β phase is much slower and reaches a maximum value of approx. 83% at a draw ratio of 8:1. It must be mentioned here that at high draw ratios beyond 7:1 in continuous production, the yarn breaks frequently. Also, on comparison of poled and unpoled samples (only drawn, without the application of electric field), a marginal change in the β-phase was observed for poled and drawn samples as shown in Fig. 1(b) and Fig. 2(b).

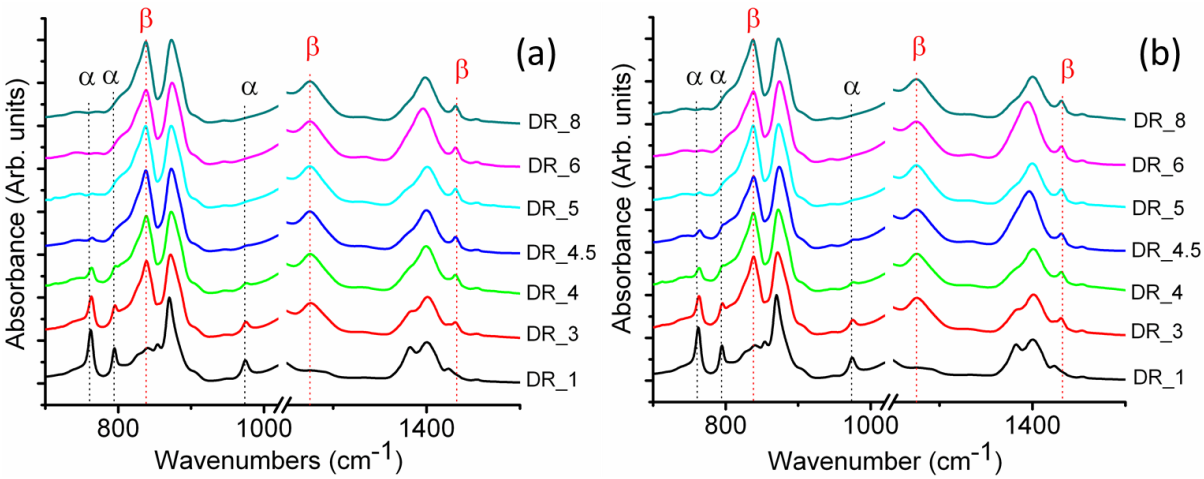

Fig. 1: FTIR spectra of (a) poled and (b) unpoled PVDF fibres drawn at different draw ratios

2. **DSC analysis of PVDF fibres at different draw ratios:**

To measure the variations in the degree of crystallinity as a function of draw ratio and poling, the samples were subjected to DSC scans, wherein the degree of crystallinity (ΔX_c) of each sample was calculated according to the equation:

$$\Delta Xc = \frac{\Delta H_m}{\Delta H_{m100}} \times 100\%$$

where ΔH_m is the melting enthalpy of the sample and ΔH_{m100} is the melting enthalpy for 100% crystalline material [3-5]. The value of ΔH_{m100} for 100 % β phase PVDF was taken to be 104.7 J/g and ΔH_m was calculated from the area of the endothermic melting peak [3-5].

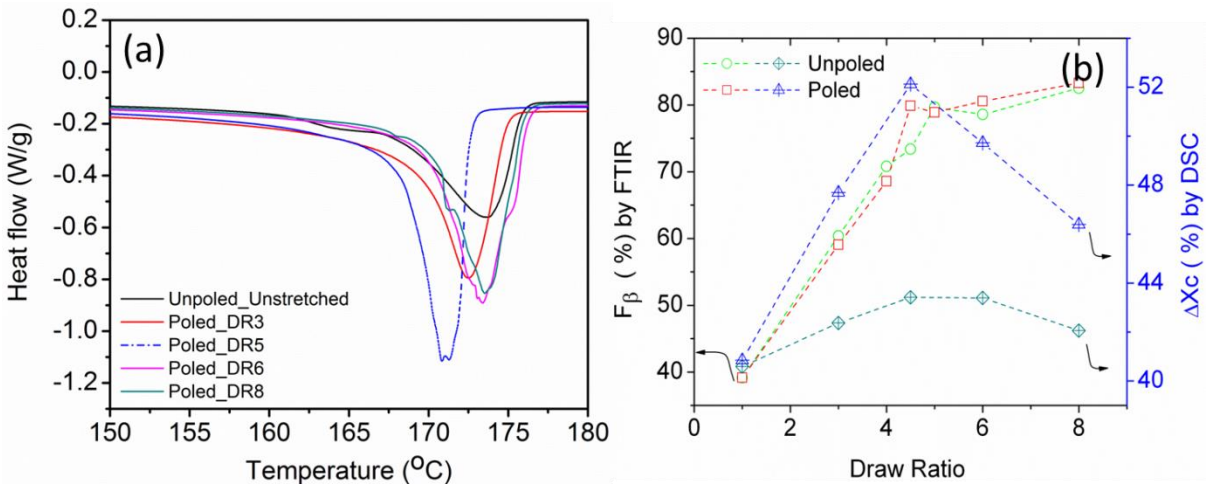

Fig. 2: (a) DSC analysis of poled PVDF samples and (b) variation of β-phase content and ΔXc as a function of draw ratio and poling.

As observed in Fig. 2(a), all the samples show an endothermic melting peak in the region of 165-175 ^{O}C with some variations in the position and width of the melting peak. The degree of crystallisation, ΔX_c for the unpoled undrawn samples was nearly the same as that of PVDF granules at 40.3 %. For PVDF granules, the melting temperature is observed at approx. 175 ^{O}C with a low degree of crystallinity, ΔX_c of the order of 38.6 %. However, upon the cold drawing and poling of the monofilament fibres, the crystallinity of the fibres is enhanced as evident by the temperature shift and the narrowing of the endotherms from nearly 175^{o} C for unpoled undrawn fibres to nearly 170 ^{O}C for poled and drawn fibres (draw ratio 5:1). Also, the degree of crystallisation, ΔX_c shows maxima for a draw ratio of 5:1 of nearly 52.1%. In fact, the ΔX_c shows a rapid increase with the increase in the drawing ratio until the draw ratio of 5:1, beyond which it starts to reduce as shown in Fig. 2(b). While the initial enhancement in the crystallinity of the monofilaments can be attributed to an increase in the β phase due to drawing and poling of the samples, the lowering of the β phase at higher drawing ratios can be attributed to various reasons. According to the theory put forward by Sajkiewicz et al. [6], the variation in the β phase can be related to the presence of a transition/initiation temperature

for the conversion of α → β phase. At this transition temperature (of nearly 65 ^{O}C, as reported by Sajkiewicz et al., [6]) the chain mobility in the disordered regions increases greatly so that the stress generated during the uniaxial drawing is transferred into the crystals to rearrange them into all trans-planar β phase. At higher draw ratios, the subsequent increase in the chain mobility mainly results in the crystal reorientation along the direction of the drawing without considerable conformal change in the crystal structure leading to the suppression of β phase. This is however in contradiction to our FTIR results, which show a nearly incremental increase in the β phase even at draw ratios above 5:1. According to Hellinckx et al [7] and Gomes et al [3] the reduction in the crystallinity suggests that the mechanism of phase transformation is associated with a melting and posterior recrystallization along the draw direction of the polymer chains within the crystallites. Also, it is noted that with the increase in the draw ratio, the endotherms get narrower implying that the crystallite distribution is much more homogeneous. Thus, on drawing, a reorganisation of the crystals occurs and the parts of the chains that belong to the interphase region become more ordered thereby becoming part of the crystalline region [8].

3. **Flexibility of 3D piezoelectric fabrics:**

Recent studies by Zeng et al [10] have indicated that the failure of simple Aluminium based sheet electrodes under cyclic compression can be attributed to the stress concentration at the edges of the impact area [1]. Moreover, under compressive impacts, the flat foil electrodes do not facilitate the occurrence of local strain gradients and associated charge generation, unlike the 3D piezoelectric fabric incorporating Ag coated PA66 electrodes. The aspects of achieving high flexibility have been addressed by fabricating a single fabric structure which incorporates flexible polymeric materials such as PVDF, Ag coated PA66 and Polyester yarns. The absence of any metal foils/metallic films makes the structure highly flexible and

the structure can be flexed quite easily (Fig. 3 below). In fact, for the 3D fabric structures, the flexural rigidity and the bending modulus tests, carried out using BSI 3356, provided values of 11.25 g/cm and 3.14 kg/cm^2, respectively. The value of bending modulus is of the same order as that of cotton based fabrics which have been reported in the literature, indicating that the fabrics are quite flexible in nature. These values are very much similar to those reported for cotton based fabrics in the literature and shows the high flexibility of the 3D piezoelectric fabrics.

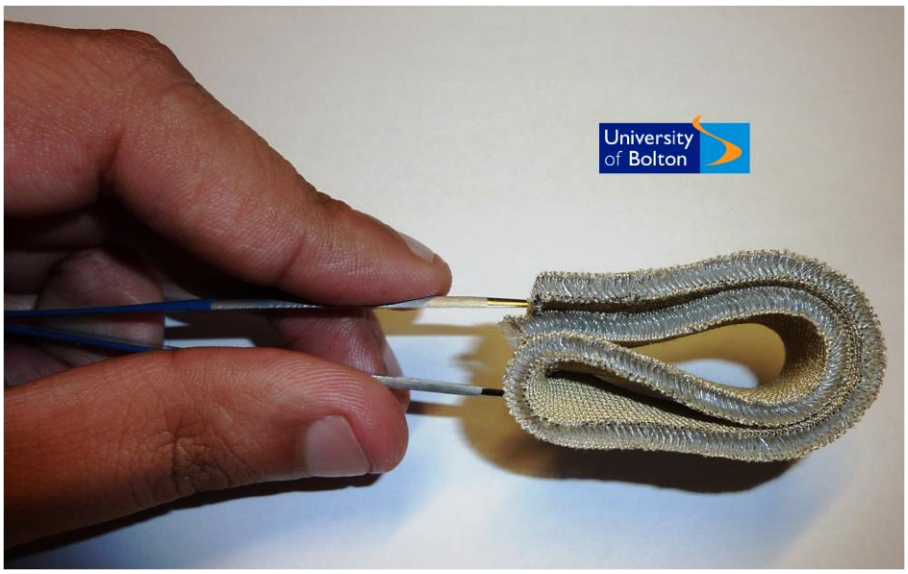

Fig. 3: Digital photograph of 3D piezoelectric fabric folded multiple times to demonstrate the flexibility of the fabric structure

4. Effect of addition of insulation yarn "Yarn B" on the compression properties of 3D piezoelectric fabrics:

The insulating yarn "Yarn B" is used to reinforce the 3D piezoelectric fabric structure. As mentioned in the main text, the maximum load that the 3D fabric (without insulating yarn) can take without the two opposite conducting faces touching each other is <0.02 MPa, which is very low. Upon the addition of insulating yarn, this maximum value of load increases to

approximately 0.13 MPa, thereby ensuring much higher energy adsorption capacity which will ultimately manifests into much more durable 3D piezoelectric textile structures.

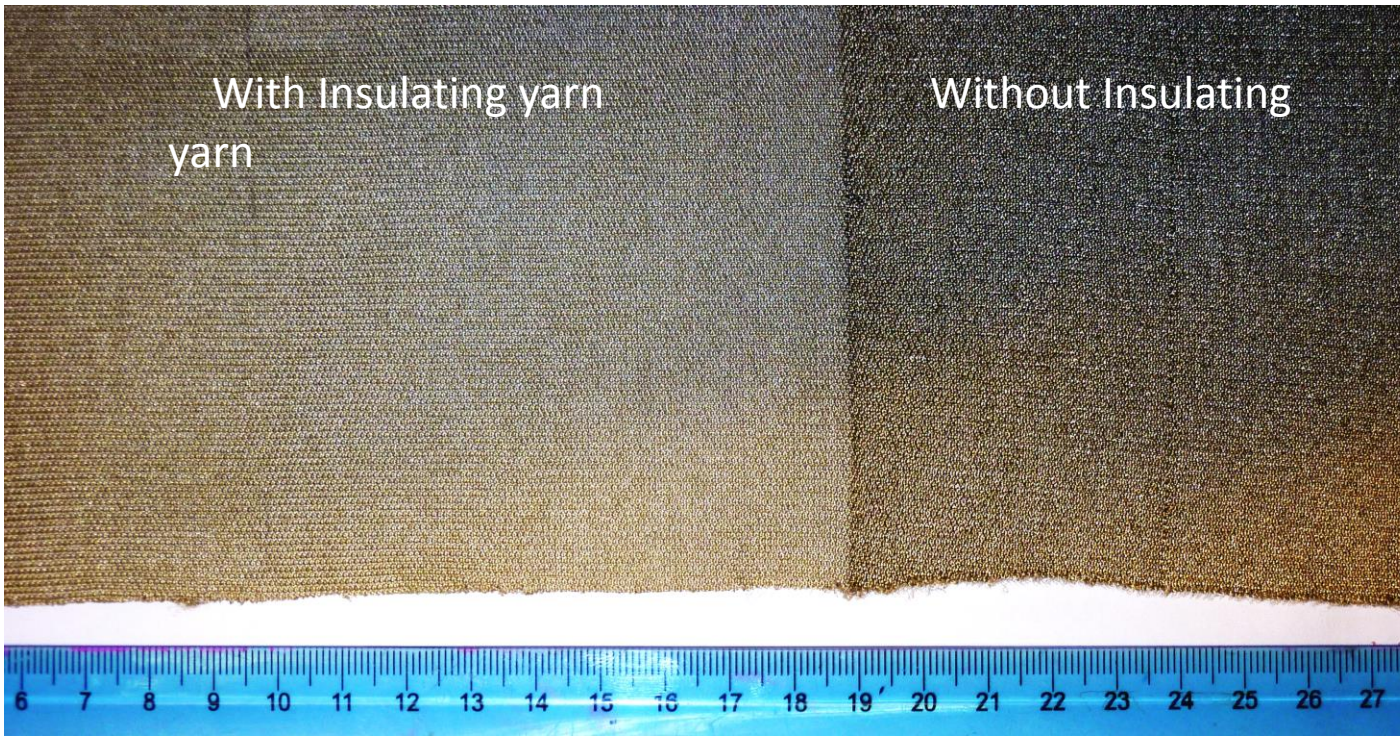

Fig. 4: Digital photograph of 3D piezoelectric fabrics with and without the insulating yarn

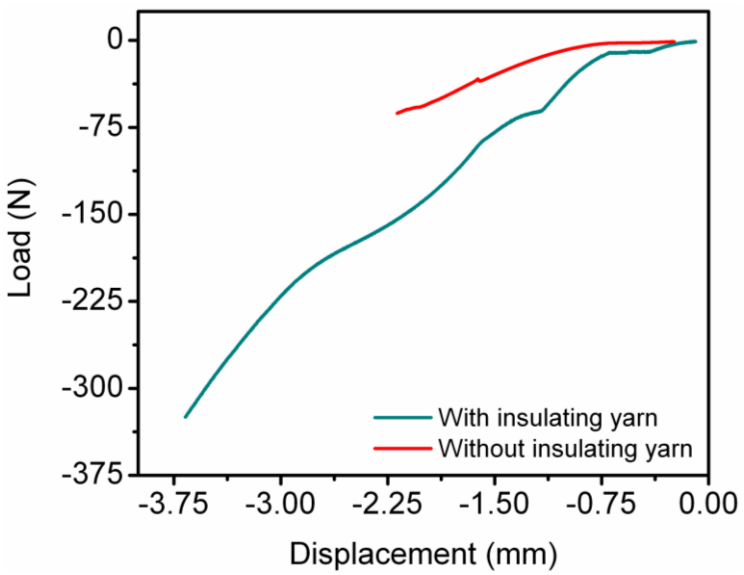

Fig. 5: Compression tests carried out on the fabric (a) with and (b) without the insulation yarn added to the 3D structure.

5. Superposition, polarity switching tests and stability tests:

To confirm that the voltage signal being obtained is from piezoelectric effect only, both the polarity-switching and superposition tests were carried out. For 3D piezoelectric fabrics, upon reversing the electrode connections, a switching in the polarity of the observed signal was observed, demonstrating that the output signal is indeed from the 3D piezoelectric fabric only rather than instrumental noise or any other artefact (see Fig. 6 below).

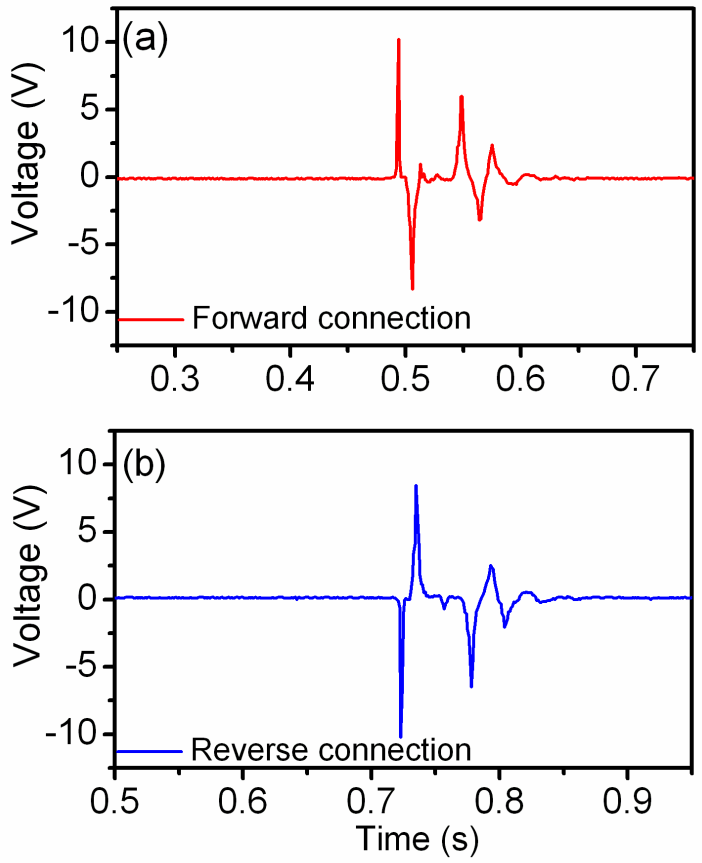

Fig. 6: Switching of the output signal on reversing the electrode connections

To observe the superposition phenomena, both the samples need to be impacted simultaneously. To this effect, instead of using two large sample sizes (15 x 5.3 cm), the samples were cut into smaller sizes of approx. 5 cm x 6 cm to accommodate under the impact tester with an applied impact pressure of ~0.02 MPa. During the impact tests, the samples were impacted simultaneously in different configurations where (a) the output of the two samples would add up and (b) the output of the two samples would cancel out each other. In

the condition where the sample output added up together a voltage of nearly 8 V was obtained (each of the samples on individual tests showed a voltage output of nearly 4.3 V each at same applied impact pressures). In the case when the samples were such connected that they would cancel out the voltage output of each other a voltage of nearly 1 V was observed as shown in Fig. 7 below.

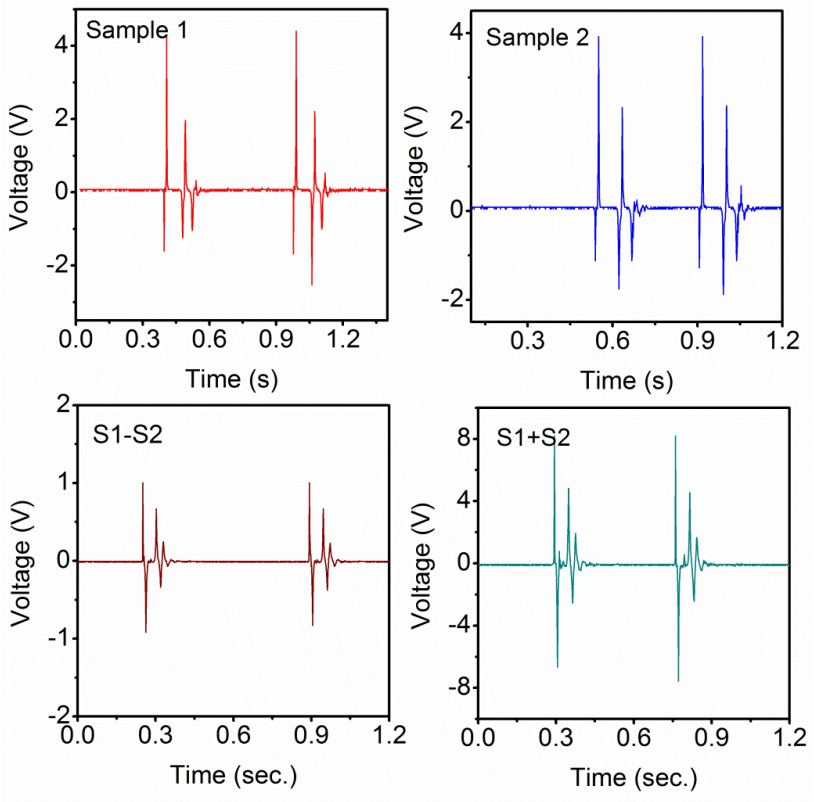

Fig. 7: Voltage response of two samples (S1, S2) and the superposition voltage output with additive effect and negating effect.

The measurements of the electrical output as a function of number of impact cycles (~ 150 cycles,) was conducted to comment on the stability of these 3D piezoelectric fabrics. It can be clearly observed that the electrical output shows very little variation of 9.93 ± 0.47V in the time duration tested.

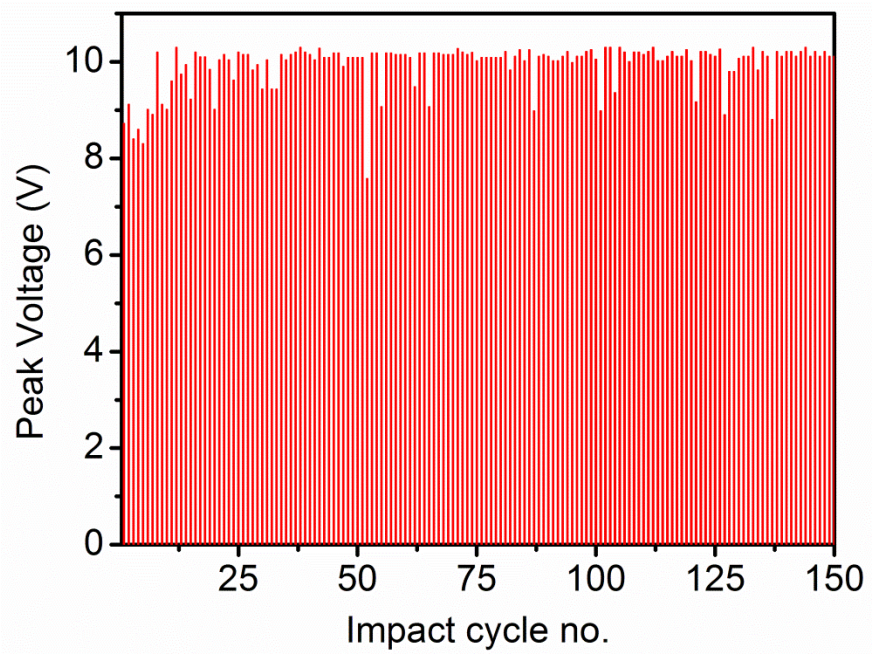

Fig. 8: Voltage response of 3D piezoelectric fabric measured over 150 test impact cycles.

6. **Power output from 2D knitted fabrics**

The as prepared PVDF monofilaments were hand knitted into fabrics on a flat V bed DUBIED NHF2 100 c/m J.36 hand-knitting machine. This knitted fabric was tested for its piezoelectric voltage response by connecting two electrodes (Electrolycra, resistance 50 Ω/m) on the opposite faces of the fabric; which were further connected to an oscilloscope. The samples were impact tested using the same conditions as that for 3D piezoelectric fabrics. The voltage and current response for the 2D knitted fabric is shown in Fig. 9.

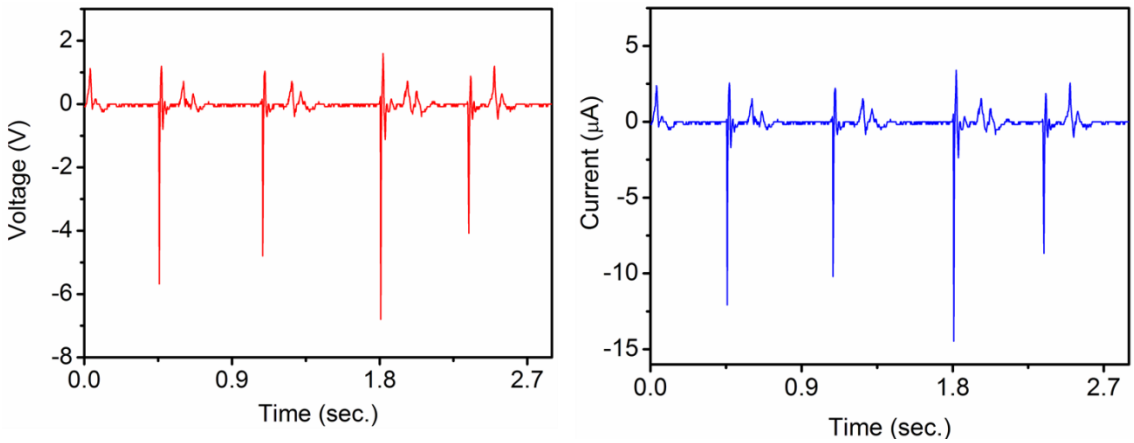

Fig. 9: Voltage and current measurement from 2D knitted fabrics

References:

[1] P. Martins, A. C. Lopes, S. Lanceros-Mendez, *Prog. Polym. Sci.* **2013,** http://dx.doi.org/10.1016/j.progpolymsci.2013.07.006

[2] A. Salimi, A. A. Yousefi, *Polym. Test.* **2003**, 22, 699

[3] J. Gomes, J. S. Nunes, V. Sencadas, S. Lanceros-Mendez, *Smart Materials and Structures*, **2010**, *19*(6), 065010

[4] R. Gregorio, M. Cestari, *J. Polym. Sci. B: Polym. Phys.* **1994**, 32, 859

[5] R. Imamura, A. B. Silva, R. Gregorio Jr, *J. Apply. Polym. Sci.* **2008,** 110, 3242

[6] P. Sajkiewicz, A. Wasiak, Z. Gocłowski, *European polymer journal*, **1999**, *35*(3), 423-429.

[7] S. Hellinckx, J. C. Bauwens, *Colloid & Polymer Science*, **1995**, *273*(3), 219-226.

[8] A. B. Silva, C. Wisniewski, J. V.A. Estevez, R. Gregorio, Ferroelectrics, **2011**, 413:1, 220-230

[9] W. Zeng, X. Tao, S. Chen, S. Shang, H. L. W. Chan, A. S. Choy, *Energy Environ. Sci.* **2013**, 6, 2631

TOC entry

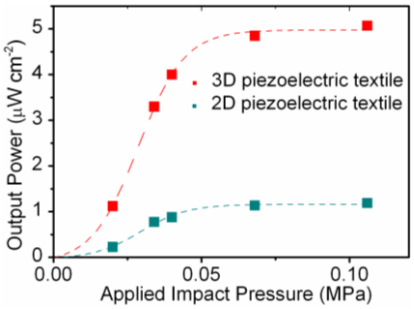

Using "3D-spacer" technology, we demonstrate novel all-fibre piezoelectric fabric power generators. The single-structure generator comprises 80% β-phase PVDF spacer monofilaments interconnected between woven Ag/PA66 electrodes. The structure provides power density of 1.10-5.10μWcm^{-2} at applied impacts of 0.02-0.10MPa, nearly five times higher than existing 2D structures.

Broader context:

The harvesting of waste energy from ambient environment and human movement has long been considered as an attractive alternative over traditional rechargeable batteries for providing electrical power to low-energy consumption devices such as wireless body worn sensors and wearable consumer electronics. However, the materials and device architectures demonstrated in the literature are not always amenable and do not provide the right "feel" and comfort level to the user. Moreover for piezoelectric application, the usage of metallic films usually limits their lifetime owing to their poor fatigue resistance to impacts. Using "3D spacer" technology, we demonstrate all-fibre flexible soft piezoelectric power generators for energy harvesting applications. A simple process utilising established knitting techniques can provide 3D piezoelectric fabric structure with integrated metallic electrodes whose flexibility is comparable to that of conventional fabrics. These 3D piezoelectric fabrics are highly suitable for applications such as wearable electronic systems, energy harvesting from human movement, body-worn sensors among others.